Monthly Notices
of the
ROYAL ASTRONOMICAL SOCIETY

Mon. Not. R. Astron. Soc. **401,** 1933–1949 (2010) doi:10.1111/j.1365-2966.2009.15781.x

# Analytical YORP torques model with an improved temperature distribution function

S. Breiter,[1⋆] D. Vokrouhlický[2] and D. Nesvorný[3]

[1]*Astronomical Observatory, A. Mickiewicz University, Sloneczna 36, PL60-286 Poznań, Poland*
[2]*Institute of Astronomy, Charles University, V Holešovičkách 2, CZ-18000, Prague 8, Czech Republic*
[3]*Department of Space Studies, Southwest Research Institute, 1050 Walnut St., Suite 300, Boulder, CO 80302, USA*

Accepted 2009 September 24. Received 2009 September 24; in original form 2009 July 14

**ABSTRACT**

Previous models of the Yarkovsky-O'Keefe-Radzievskii-Paddack (YORP) effect relied either on the zero thermal conductivity assumption, or on the solutions of the heat conduction equations assuming an infinite body size. We present the first YORP solution accounting for a finite size and non-radial direction of the surface normal vectors in the temperature distribution. The new thermal model implies the dependence of the YORP effect in rotation rate on asteroids conductivity. It is shown that the effect on small objects does not scale as the inverse square of diameter, but rather as the first power of the inverse.

**Key words:** errata, addenda – radiation mechanisms: thermal – methods: analytical – celestial mechanics – minor planets, asteroids.

## 1 INTRODUCTION

The Yarkovsky-O'Keefe-Radzievskii-Paddack (YORP) effect is considered one of the principal factors influencing the rotation of minor objects like asteroids or meteoroids (Bottke et al. 2006). Modelling the YORP torque is a complicated task, both for numerical and analytical approach. The present paper extends an analytical solution of Breiter & Michalska (2008) by introducing an improved model of the surface temperature. Using the approximate insolation function expressions of Breiter & Michalska (2008), reminded in Section 3, we derive the linearized temperature model (Section 4) that accounts for the finite size of an object and does not assume the radial direction of the surface normal in the part of boundary conditions related with the heat conduction. The mean values of dynamically significant YORP torque projections are derived in Section 6 in a general form. Their limits at large and small values of an object's radius are given in Sections 7 and 8. An exemplary application to the asteroid 1998 KY26 with different physical properties and size is presented in Section 9. The most important conclusion of our work are the dependence of the YORP effect in rotation period on the conductivity, and the change of the scale factor from the inverse square of diameter to the first power of the inverse, occurring for smaller objects.

Certain ambiguity in the definition of the YORP effect originates from the fact, that Lambertian scattering of incoming light flux can be described by the formulae that are very similar to the thermal reradiation case, except for their independence on conductivity. In most of the present paper, we consider the YORP effect as a phenomenon caused by thermal reradiation. Only in the Appendix A we consider both phenomena simultaneously.

The present paper uses the same formalism as Breiter & Michalska (2008) and required re-derivation of its results as a limit case. The errors discovered in Breiter & Michalska (2008) are listed in Appendix B.

## 2 GENERAL FORMULA FOR THE YORP TORQUE

Using common assumptions of the Lambert emission model and the homogeneity of an asteroid's surface properties, we express the YORP torque as a surface integral (e.g. Bottke et al. 2006):

$$\boldsymbol{M} = -\frac{2}{3}\frac{\varepsilon_{\rm t}\sigma}{c}\oint_S T^4\,(\boldsymbol{r}\times{\rm d}\boldsymbol{S}), \tag{1}$$

where $\varepsilon_{\rm t}$ is the surface emissivity, $\sigma$ is the Stefan–Boltzmann constant, $c$ designates the velocity of light and $T$ is the surface temperature – a function of the longitude, latitude and of the Sun position. It should be observed that the general formula (1) contains two concurrent factors: one related to the non-spherical shape, vanishing identically when $\boldsymbol{r}\times{\rm d}\boldsymbol{S}=\boldsymbol{0}$, and another one related to temperature. Was $T$ independent

⋆E-mail: breiter@amu.edu.pl

on coordinates, one might pull it out of the integrand and then $\oint_S \boldsymbol{r} \times \mathrm{d}\boldsymbol{S} = \boldsymbol{0}$, regardless of the time dependence of $T$? In other words, isothermal bodies are not YORP torqued [see Breiter & Michalska (2008) for a different formulation of this property].

## 3 BODY SHAPE MODEL AND INSOLATION FUNCTION

### 3.1 Surface equation and normal vectors

The body shape can be specified in terms of the colatitude $\theta$ and longitude $\lambda$ measured in the reference frame with the origin at the centre of mass and the axes aligned with the principal axes of inertia (the body frame). Assuming the spherical harmonics series form, the shape is defined by the reference radius $a$ and a set of shape coefficients: either real $C_{l,m}, S_{l,m}$ or complex $f_{l,m}$, up to the maximum degree and order of $N$:

$$R = a + a \sum_{l=1}^{N} \sum_{m=0}^{l} \Theta_l^m(\cos\theta)[C_{l,m}\cos m\lambda + S_{l,m}\sin m\lambda] = a + a \sum_{l\geq 1} \sum_{m=-l}^{l} f_{l,m} Y_{l,m}, \tag{2}$$

where $\Theta_l^m(u)$ are the normalized Legendre functions

$$\Theta_l^m(u) = \sigma_{l,m} P_l^m(u), \tag{3}$$

that differ from the usual associated Legendre functions $P_l^m(u)$,

$$P_l^m(u) = \frac{(-1)^m}{2^l\, l!} (1-u^2)^{\frac{m}{2}} \frac{\mathrm{d}^{l+m}(u^2-1)^l}{\mathrm{d}u^{l+m}} = (-1)^m (1-u^2)^{\frac{m}{2}} \frac{\mathrm{d}^m P_l(u)}{\mathrm{d}u^m}, \tag{4}$$

by the normalizing factor $\sigma_{l,m}$

$$\sigma_{l,m} = \sqrt{\frac{2l+1}{4\pi} \frac{(l-m)!}{(l+m)!}}. \tag{5}$$

Complex spherical harmonics $Y_{l,m} = Y_{l,m}(u,\lambda)$ used in this paper are defined as

$$Y_{l,m}(u,\lambda) = \Theta_l^m(u)\, \mathrm{e}^{\mathrm{i}\, m\, \lambda}. \tag{6}$$

The symbols $u$ and $w$ in the following text will always mean

$$u = \cos\theta, \quad w = \sin\theta = \sqrt{1-u^2}. \tag{7}$$

The real and complex shape coefficients are related by $f_{l,0} = C_{l,0}$ and, for $m > 0$,

$$\begin{aligned} f_{l,m} &= (C_{l,m} - \mathrm{i}\, S_{l,m})/2, \\ f_{l,-m} &= (-1)^m\, (C_{l,m} + \mathrm{i}\, S_{l,m})/2 = (-1)^m\, f_{l,m}^*, \\ C_{l,m} &= \left[f_{l,m} + (-1)^m f_{l,-m}\right] = f_{l,m} + f_{l,m}^*, \\ S_{l,m} &= \mathrm{i}\, \left[f_{l,m} - (-1)^m f_{l,-m}\right] = \mathrm{i}\,(f_{l,m} - f_{l,m}^*). \end{aligned} \tag{8}$$

Using a real-valued sum

$$\Psi = \sum_{l\geq 1} \sum_{m=-l}^{l} f_{l,m} Y_{l,m}, \tag{9}$$

considered as small quantity of a first order, we can replace equation (2) by an abbreviated form

$$R = a\,(1+\Psi). \tag{10}$$

Similar to Breiter & Michalska (2008), we use a modified set of spherical coordinates with a right-handed, orthonormal basis:

$$\begin{aligned} \hat{\boldsymbol{e}}_r &= (w\,\cos\lambda,\ w\,\sin\lambda,\ u)^{\mathrm{T}}, \\ \hat{\boldsymbol{e}}_\lambda &= \frac{1}{w} \frac{\partial \hat{\boldsymbol{e}}_r}{\partial \lambda} = (-\sin\lambda,\ \cos\lambda,\ 0)^{\mathrm{T}}, \\ \hat{\boldsymbol{e}}_u &= w \frac{\partial \hat{\boldsymbol{e}}_r}{\partial u} = (-u\,\cos\lambda,\ -u\,\sin\lambda,\ w)^{\mathrm{T}}. \end{aligned} \tag{11}$$

In terms of the spherical surface gradient $\nabla_{\mathrm{s}}$,

$$\nabla_{\mathrm{s}} f \equiv \frac{1}{w} \frac{\partial f}{\partial \lambda} \hat{\boldsymbol{e}}_\lambda + w \frac{\partial f}{\partial u} \hat{\boldsymbol{e}}_u. \tag{12}$$

We can define the outward normal vector $\boldsymbol{N}$ as in (Breiter & Michalska 2008),

$$\boldsymbol{N} = \frac{\partial \boldsymbol{r}}{\partial \lambda} \times \frac{\partial \boldsymbol{r}}{\partial u} = a^2\,(1+\Psi)\,[(1+\Psi)\,\hat{\boldsymbol{e}}_r - \nabla_{\mathrm{s}}\Psi], \tag{13}$$

and the first order approximation of its unit vector is

$$\hat{\boldsymbol{n}} = \frac{\boldsymbol{N}}{N} \approx \hat{\boldsymbol{e}}_r - \nabla_{\mathrm{s}}\Psi. \tag{14}$$

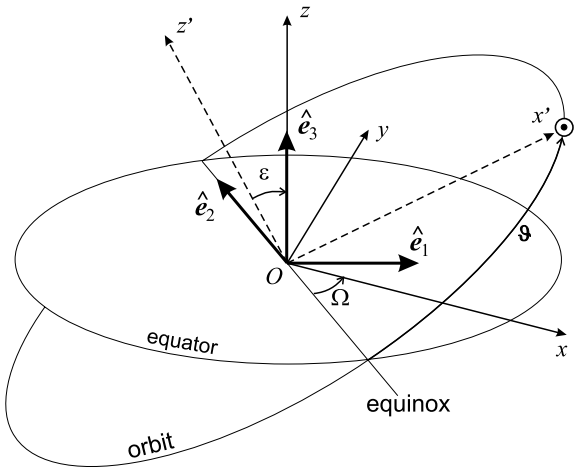


**Figure 1.** Reference frames and orientation angles.

### 3.2 Solar position and insolation function

Similarly to Breiter & Michalska (2008), we use two sets of Euler angles to define the rotation from the body frame $Oxyz$ to the orbital frame $Ox'y'z'$ ($Ox'$ directed to the Sun, $Oz'$ along the orbital momentum and $Oy'$ axis completing the orthogonal, right-handed triad): 3-1-3 angles $\Omega, \varepsilon, \vartheta$ and 3-2-3 angles $\phi, \varepsilon, \psi$ (see Fig. 1). In terms of rotation matrices $\mathbf{R}_i$,

$$\boldsymbol{r}' = \mathbf{R}_3(\vartheta)\mathbf{R}_1(\varepsilon)\mathbf{R}_3(-\Omega)\,\boldsymbol{r} = \mathbf{R}_3(\psi)\mathbf{R}_2(\varepsilon)\mathbf{R}_3(\phi)\,\boldsymbol{r}, \tag{15}$$

with the equivalence condition

$$\phi = -\Omega - \frac{\pi}{2}, \quad \psi = \vartheta + \frac{\pi}{2}. \tag{16}$$

Thus, the unit vector directed to the Sun is given in the body frame as

$$\hat{\boldsymbol{n}}_\odot = (c\,\cos\phi\,\cos\psi - \sin\phi\sin\psi)\,\hat{\boldsymbol{e}}_x + (c\,\sin\phi\,\cos\psi + \cos\phi\sin\psi)\,\hat{\boldsymbol{e}}_y - s\,\cos\psi\,\hat{\boldsymbol{e}}_z, \tag{17}$$

where

$$c = \cos\varepsilon, \quad s = \sin\varepsilon \tag{18}$$

are related with the obliquity angle $\varepsilon$. Further, we consider $\varepsilon$ (hence $c$ and $s$) a constant quantity, so the motion of the Sun in the body frame consists of the yearly and daily motions due to the increasing $\psi$ and $\phi$, respectively.

The primary definition of the insolation function $\mathcal{E}$ is given by

$$\mathcal{E} = (1 - A)\,\Phi\,\max(0, \hat{\boldsymbol{n}} \cdot \hat{\boldsymbol{n}}_\odot), \tag{19}$$

where $A$ is the Bond albedo and $\Phi$ designates the solar radiation energy flux. Using the distance of the body from the Sun $r_\mathrm{o}$ and the solar constant $\Phi_0 \approx 1366\ \mathrm{W\,m^{-2}}$, one computes $\Phi$ as

$$\Phi = \Phi_0 \left(\frac{d_0}{r_\mathrm{o}}\right)^2, \tag{20}$$

with the reference distance $d_0 = 1$ au. Note that $\mathcal{E}$ describes only the direct insolation, i.e. we neglect the illumination by the light reflected by other surface fragments. Moreover, we ignore the shadows cast by the parts of an object that stretch above the local tangent plane. In other words, for the purpose of computing the insolation, we treat the body shape as a convex surface.

Requiring the spherical harmonics series of the insolation function for the derivation of the thermal model, we use the first order approximation derived in Breiter & Michalska (2008):

$$\mathcal{E} \approx \mathcal{E}_0 + \mathcal{E}_1 = \sum_{l\geqslant 0}\sum_{m=-l}^{l}\left(\mathcal{E}^{(0)}_{l,m} + \mathcal{E}^{(1)}_{l,m}\right) Y_{l,m}, \tag{21}$$

where

$$\mathcal{E}^{(0)}_{l,m} = -(1 - A)\,\Phi \sum_{k=-l}^{l} \frac{H_k\, w^{1,k}_{1,l}}{\sigma_{1,1}}\, D^l_{m,k}, \tag{22}$$

$$\mathcal{E}^{(1)}_{l,m} = (-1)^m\,(1 - A)\,\Phi \sum_{j\geqslant 1}\sum_{k=-j}^{j} f_{j,k} \sum_{p=0}^{l+j} g^l_{p,j}\, \mathcal{G}^{m-k,k,-m}_{p,j,l} \sum_{q=-p}^{p} \frac{H_q\, w^{1,q}_{1,p}}{\sigma_{1,1}}\, D^p_{m-k,q}. \tag{23}$$

Apart from Wigner functions (Biedenharn & Louck 1981),

$$D^l_{m,k} = d^l_{m,k}(\varepsilon)\,\mathrm{e}^{-\mathrm{i}(m\phi + k\,\psi)}, \tag{24}$$

the above expressions involve two ad hoc symbols:

$$g^{l}_{p,j} = \frac{1}{2}\,[p\,(p+1) + j\,(j+1) - l\,(l+1)]\,, \tag{25}$$

$$H_q = \int_{-\frac{\pi}{2}}^{\frac{\pi}{2}} \cos L\ \mathrm{e}^{\mathrm{i}qL}\,\mathrm{d}L, \tag{26}$$

and more common special functions, like overlap integrals,

$$w^{m_1,m_2}_{n_1,n_2} = \int_{-1}^{1} \Theta^{m_1}_{n_1}(u)\,\Theta^{m_2}_{n_2}(u)\,\mathrm{d}u, \tag{27}$$

and Gaunt coefficients

$$\mathcal{G}^{m_1,m_2,m_3}_{l_1,l_2,l_3} = \int_{-1}^{1}\mathrm{d}u \int_{0}^{2\pi} Y_{l_1,m_1}(u,\lambda)\,Y_{l_2,m_2}(u,\lambda)\,Y_{l_3,m_3}(u,\lambda)\,\mathrm{d}\lambda. \tag{28}$$

More details can be found in section 3 and appendix A of Breiter & Michalska (2008).

## 4 TEMPERATURE MODEL

### 4.1 General solution

In the so-called Rubincam's approximation (Rubincam 2000; Vokrouhlický & Čapek 2002), when the thermal conductivity $K$ is negligible, the temperature distribution is described by

$$T^4 = \frac{\mathcal{E}}{\varepsilon_{\mathrm{t}}\,\sigma}, \tag{29}$$

where $\mathcal{E}$ is the insolation function. But if the conductivity $K$ cannot be neglected, a more realistic temperature model should be adopted, based upon the solution of the heat diffusion equation. Assuming a homogeneous body with constant thermal parameters, we use the Fourier equation. If we express the Laplacian operator in a modified set of spherical variables $r, u, \lambda$, the equation takes the form

$$\frac{\partial T}{\partial t} = \frac{\kappa}{r^2}\left\{\frac{\partial}{\partial r}\left(r^2\,\frac{\partial T}{\partial r}\right) + \frac{\partial}{\partial u}\left[(1-u^2)\,\frac{\partial T}{\partial u}\right] + \frac{1}{1-u^2}\,\frac{\partial^2 T}{\partial \lambda^2}\right\} = \frac{\kappa}{r^2}\left[\frac{\partial}{\partial r}\left(r^2\,\frac{\partial T}{\partial r}\right) + \Delta_{\mathrm{s}} T\right], \tag{30}$$

where $\Delta_{\mathrm{s}}$ designates the Laplace operator restricted to the unit sphere, and $\kappa$ is the ratio of the thermal conductivity to the product of the density $\rho$ and the specific heat capacity $c_{\mathrm{p}}$,

$$\kappa = \frac{K}{\rho\,c_{\mathrm{p}}}. \tag{31}$$

The general solution of the linear equation (30), non-singular at $r = 0$, is known to be the superposition of terms

$$T_{l,m,\beta} = j_l(\beta\,r)\,Y_{l,m}(u,\lambda)\,\mathrm{e}^{-\kappa\beta^2 t}, \tag{32}$$

where $l, m$ and $\beta$ are the arbitrary separation constants, and $j_l$ designates a spherical Bessel function of the first kind, related to the ordinary Bessel function $J_\nu$ through

$$j_l(x) = \sqrt{\frac{\pi}{2x}}\,J_{l+\frac{1}{2}}(x). \tag{33}$$

Restricting the separation constants $l$ and $m$ to integer values $l \geqslant 0$, and $-l \leqslant m \leqslant l$, we obtain all terms $T_{l,m,\beta}$ non-singular for $r \geqslant 0$, and $2\pi$-periodic in $\lambda$.

However, the solution (32) is based upon a hidden assumption that $\beta \neq 0$, and one may easily verify that it degenerates into $T_{l,m,0} = Y_{0,0}$ when the separation constant is set to $\beta = 0$. But the time independent temperature obeys the Laplace equation $\Delta T = 0$, with a non-trivial classical solution $T_{l,m,0} = (r/a_{\mathrm{s}})^l Y_{l,m}(u,\lambda)$ where $a_{\mathrm{s}}$ is a scaling parameter with the dimension of length, most conveniently – the mean radius of the body $a$. Thus, we enrich equation (32) and replace it by

$$T_{l,m,\beta} = E_l(\beta, r)\,Y_{l,m}(u,\lambda)\,\mathrm{e}^{-\kappa\beta^2 t}, \tag{34}$$

where

$$E_l(\beta, r) = \begin{cases} \left(\frac{r}{a}\right)^l, & \text{for } \beta = 0, \\ j_l(\beta\,r), & \text{for } \beta \neq 0. \end{cases} \tag{35}$$

A difficult part of determining the temperature is the choice of $\beta$ and of the arbitrary constants for the superposition of $T_{l,m,\beta}$. It has to be done according to the boundary conditions on the body surface, where the conservation of energy implies

$$\left[\varepsilon_{\mathrm{t}}\,\sigma\,T^4 + K\,\hat{\boldsymbol{n}}\cdot\nabla T\right]_{r=R} - \mathcal{E} = 0. \tag{36}$$

The first term is the reradiated energy, proportional to the fourth power of $T$, and the product of the Stefan–Boltzmann constant $\sigma$ and the surface emissivity $\varepsilon_{\mathrm{t}}$. The second term is responsible for the heat absorption, and the last term is the incoming radiation energy $\mathcal{E}$, known as the insolation function. Moreover, we search only the solution that is a quasi-periodic function of time.

### 4.2 Linearized temperature model

#### *4.2.1 Linearized boundary conditions*

The boundary conditions (36) are non-linear, so we follow a common practice of linearizing the temperature, by assuming $T = T_0 + T_1$, with time and coordinates independent $T_0$, and a correction $T_1$. Instead of adopting the most popular 'plane parallel' model, based on the assumption that $\hat{\boldsymbol{n}} \cdot \nabla T \approx \hat{\boldsymbol{e}}_r \cdot \nabla T$, we inspect a more elaborate approach with non-radial normal vector in equation (36).

In terms of the unit vectors (11), we can express the gradient of $T$ at the surface as

$$\nabla T = \left[ \frac{\partial T}{\partial r}\, \hat{\boldsymbol{e}}_r + \frac{1}{r\, w}\, \frac{\partial T}{\partial \lambda}\, \hat{\boldsymbol{e}}_\lambda + \frac{w}{r}\, \frac{\partial T}{\partial u}\, \hat{\boldsymbol{e}}_u \right]_R = \left[ \frac{\partial T}{\partial r}\, \hat{\boldsymbol{e}}_r + \frac{1}{r}\, \nabla_{\rm s} T \right]_R , \tag{37}$$

whereas the linear approximation of the unit normal vector $\hat{\boldsymbol{n}}$ on the surface is already known from equation (14). Thus,

$$\hat{\boldsymbol{n}} \cdot \nabla T \approx \left[ \frac{\partial T}{\partial r} - \frac{1}{r}\, \nabla_{\rm s} T \cdot \nabla_{\rm s} \Psi \right]_R . \tag{38}$$

Introducing the second term from the right-hand side of (38) in the boundary condition (36) is a novelty of our approach that enables us to go beyond the plane parallel approximation, characteristic to all previous analyses of the YORP effect.

Setting $T = T_0 + T_1$, in the boundary conditions (36), and linearizing with respect to $T_1$, we first obtain

$$\varepsilon_{\rm t}\, \sigma\, T_0^4 = \mathcal{E}_0^{\rm c} = \frac{(1 - A)\, \Phi}{4}, \tag{39}$$

$$\left[ 4\, \varepsilon_{\rm t}\, \sigma\, T_0^3\, T_1 + K\, \hat{\boldsymbol{n}} \cdot \nabla T_1 \right]_R = \mathcal{E} - \mathcal{E}_0^{\rm c}. \tag{40}$$

In order to handle equation (40), we observe that according to (38) the product $\hat{\boldsymbol{n}} \cdot \nabla T_1$ is the sum of a radial derivative $\frac{\partial T_1}{\partial r}$ and of a term resulting from the deviation of $\hat{\boldsymbol{n}}$ from the radial direction. Assuming the latter to be a small quantity, we resort to the perturbation approach by introducing $T_1 = \widetilde{T}_{1,0} + \widetilde{T}_{1,1}$, where the second subscript distinguishes the values implied by a spherical part of the insolation function $\widetilde{T}_{1,0}$, and corrections due to non-spherical terms in both the insolation function and the derivative along the normal vector $\widetilde{T}_{1,1}$. In these circumstances, we partition equation (40) and replace it by two boundary conditions

$$\left[ 4\, \varepsilon_{\rm t}\, \sigma\, T_0^3\, \widetilde{T}_{1,0} + K\, \frac{\partial \widetilde{T}_{1,0}}{\partial r} \right]_R = \mathcal{E}_0 - \mathcal{E}_0^{\rm c}, \tag{41}$$

$$\left[ 4\, \varepsilon_{\rm t}\, \sigma\, T_0^3\, \widetilde{T}_{1,1} + K\, \frac{\partial \widetilde{T}_{1,1}}{\partial r} \right]_R = \mathcal{E}_1 + \mathcal{E}_{1,1}, \tag{42}$$

where

$$\mathcal{E}_{1,1} = \left[ \frac{K}{r}\, \nabla_{\rm s} \widetilde{T}_{1,0} \cdot \nabla_{\rm s} \Psi \right]_R . \tag{43}$$

As usually in perturbation theory, equations (41) and (42) have the same structure and differ only by the source terms on their right-hand side. Both solution terms $\widetilde{T}_{1,0}$ and $\widetilde{T}_{1,1}$ are superpositions of expression (34) and the final outcome should result in

$$\varepsilon_{\rm t} \sigma T^4 \approx \varepsilon_{\rm t} \sigma \left( T_0^4 + 4 T_0^3 \widetilde{T}_{1,0} + 4 T_0^3 \widetilde{T}_{1,1} \right), \tag{44}$$

appearing as a factor in the YORP torque definition.

The reason for introducing tildes over the two temperature terms is to distinguish their temporary character as the functions of $R$. Later on, when we substitute $R = a(1 + \Psi)$, they will generate the final $T_{1,0}$ and $T_{1,1}$, being the functions of the mean radius $a$.

#### *4.2.2 General patterns*

The first term, $\varepsilon_{\rm t} \sigma T_0^4$, is explicitly given by equation (39), but equations (41) and (42) are more complicated. The complete solution of the heat diffusion equation is a superposition of general terms (34). In case of linearized boundary conditions, the coefficients of the linear combination of the terms can be determined one by one; anticipating the form implied by the insolation function $\mathcal{E}$ present in the boundary conditions, we assume $T_1$ composed of terms

$$\widetilde{T}_{l,m,p,q} = C_{l,m,p,q}\, E_l(\beta, r)\, Y_{l,m}(u, \lambda)\, {\rm e}^{-\beta^2 \kappa t + {\rm i}\, \delta_{p,q}}, \tag{45}$$

which means that the coefficients to be determined are $C_{l,m,p,q} {\rm e}^{{\rm i}\, \delta_{p,q}}$, where each pair $(p, q)$ refers to some value of $\beta$.

Beginning with the simple case of $p = q = 0$, we substitute (45) into (41) or (42) with the right-hand side consisting of a single term of the insolation function series. This leads to

$$C_{l,m,0,0} \left( \frac{R}{a} \right)^l \left[ 4\, \varepsilon_{\rm t} \sigma T_0^3 + K\, l\, R^{-1} \right] Y_{l,m}\, {\rm e}^{{\rm i}\, \delta_{0,0}} = B_{l,m,0,0}\, Y_{l,m}, \tag{46}$$

and so, setting $\delta_{0,0} = 0$, we find

$$4\, \varepsilon_{\rm t}\, \sigma\, T_0^3\, \widetilde{T}_{l,m,0,0} = B_{l,m,0,0} J_{0,0}^l(R)\, Y_{l,m}, \tag{47}$$

where

$$J^l_{0,0}(R) = \frac{1}{1 + l\,\frac{\gamma}{R}}, \tag{48}$$

with

$$\gamma = \frac{K}{4\,\varepsilon_{\rm t}\,\sigma\,T_0^3}. \tag{49}$$

The time-dependent case is more involved. This time, the substitution of (45) results in the boundary condition

$$C_{l,m,p,q}\,\left[4\,j_l(\beta R)\,\varepsilon_{\rm t}\sigma T_0^3 + K\beta\,j_l'(\beta R)\right]\,Y_{l,m}\,{\rm e}^{-\kappa\beta^2\,t+{\rm i}\,\delta_{p,q}} = B_{l,m,p,q}\,Y_{l,m}\,{\rm e}^{{\rm i}\,(p\phi+q\,\psi)}, \tag{50}$$

where $j_l'(z) = \frac{{\rm d}j_l(z)}{{\rm d}z}$.

The time dependence of the right-hand side of equation (50) is encapsulated in

$${\rm e}^{{\rm i}\,(p\phi+q\,\psi)} = {\rm e}^{{\rm i}\,(p\,\dot\phi+q\,\dot\psi)\,t+{\rm i}[p\,\phi(0)+q\,\psi(0)]} = {\rm e}^{-{\rm i}\,(p\,\omega-q\,n_{\rm s})\,t+{\rm i}[p\,\phi(0)+q\,\psi(0)]}, \tag{51}$$

provided a uniform rotation with frequency $\omega$ and a circular orbit with the mean motion $n_{\rm s}$ are assumed for the asteroid, and the values of angles at $t = 0$ are $\phi(0)$ and $\psi(0)$. Comparing (51) with the exponential in the left-hand side of (50), we conclude

$$\beta^2 = {\rm i}\,\frac{p\omega - q\,n_{\rm s}}{\kappa}, \tag{52}$$

so $\beta$ must be a complex quantity

$$\beta = \pm\left[1 + b_{p,q}\,{\rm i}\right]\,\sqrt{\frac{|p\omega - q\,n_{\rm s}|}{2\,\kappa}}, \quad b_{p,q} = {\rm sgn}(p\omega - qn_{\rm s}). \tag{53}$$

Without loosing generality, we may focus on the plus sign choice in equation (53), and introduce two auxiliary quantities

$$\beta_{p,q} = \beta_{-p,-q} = \sqrt{\frac{|p\omega - qn_{\rm s}|}{2\kappa}}, \tag{54}$$

$$Z_{p,q} = (1 + {\rm i}b_{p,q})\,\beta_{p,q}. \tag{55}$$

Identifying

$$\delta_{p,q} = p\,\phi(0) + q\,\psi(0), \tag{56}$$

we find a generic boundary condition

$$4\,\varepsilon_{\rm t}\,\sigma\,T_0^3\,C_{l,m,p,q}\,j_l(Z_{p,q}\,R)\,\left[1 + \gamma\,Z_{p,q}\,\frac{j_l'(Z_{p,q}\,R)}{j_l(Z_{p,q}\,R)}\right] = B_{l,m,p,q}. \tag{57}$$

Using a complex quantity

$$J^l_{p,q}(R) = \frac{1}{1 + \gamma\,Z_{p,q}\,\frac{j_l'(Z_{p,q}\,R)}{j_l(Z_{p,q}\,R)}}, \tag{58}$$

we obtain

$$4\,\varepsilon_{\rm t}\,\sigma\,T_0^3\,C_{l,m,p,q}\,j_l(Z_{p,q}\,R) = B_{l,m,p,q}\,J^l_{p,q}(R). \tag{59}$$

So the solution of a time dependent boundary condition (50) is

$$4\,\varepsilon_{\rm t}\,\sigma\,T_0^3\,\widetilde{T}_{l,m,p,q} = B_{l,m,p,q}J^l_{p,q}(R)\,Y_{l,m}\,{\rm e}^{{\rm i}\,(p\phi+q\psi)}. \tag{60}$$

In the following considerations, we will use the general form (60), bearing in mind that $J^l_{p,q}(R)$ may have a different form (58) or (48) depending on the values of indices $p$ and $q$. Note that changing the signs of both subscripts is equivalent to taking the complex conjugate of the $J$ function, i.e.

$$J^l_{-p,-q} = J^{l\,*}_{p,q}. \tag{61}$$

#### *4.2.3 Linear solution coefficients as the functions of R*

Equation (60) can be immediately applied to the condition (41), where $\mathcal{E}_0$ is given by (22), resulting in

$$4\,\varepsilon_{\rm t}\,\sigma\,T_0^3\,\widetilde{T}_{1,0} = \sum_{l\geqslant 1}\,\sum_{m=-l}^{l}\,\tau^{(0)}_{l,m}\,Y_{l,m}, \tag{62}$$

where

$$\tau^{(0)}_{l,m} = -(1 - A)\,\Phi\,\sum_{k=-l}^{l}\,\frac{w^{1,k}_{1,l}\,H_k}{\sigma_{1,1}}\,J^{l\,*}_{m,k}(R)\,D^l_{m,k}. \tag{63}$$

In order to find the non-spherical contribution $\widetilde{T}_{1,1}$, we inspect the two separate source terms appearing in the right-hand sides of equation (42): $\mathcal{E}_1$ and $\mathcal{E}_{1,1}$ generating, respectively, the two components of

$$\tau_{l,m}^{(1)} = \tau_{l,m}^{(10)} + \tau_{l,m}^{(11)} \tag{64}$$

in

$$4\,\varepsilon_{\rm t}\,\sigma\,T_0^3\,\widetilde{T}_{1,1} = \sum_{l\geqslant 0}\sum_{m=-l}^{l}\tau_{l,m}^{(1)}\,Y_{l,m}. \tag{65}$$

The first one, $t_{l,m}^{(10)}$, stems directly from the insolation function part $\mathcal{E}_1$ listed in equation (23). Thus, straightforward application of the rule (60) leads to

$$\tau_{l,m}^{(10)} = (-1)^m\,(1-A)\,\Phi\sum_{j\geqslant 1}\sum_{k=-j}^{j} f_{j,k}\sum_{p=0}^{l+j} g_{p,\,j}^{l}\,\mathcal{G}_{p,j,l}^{m-k,k,-m}\sum_{q=-p}^{p}\frac{H_q\,w_{1,p}^{1,q}}{\sigma_{1,1}}\,J_{m-k,q}^{l\,*}(R)\,D_{m-k,q}^{p}. \tag{66}$$

The second, $\tau_{l,m}^{(11)}$, caused by the deviation of normal vector from the radial direction, can be most easily derived by making use of to the properties of the gradient on unit sphere $\nabla_{\rm s}$. Using the identities of vector analysis, we can rewrite equation (43) in terms of the Laplace operator on unit sphere:

$$\mathcal{E}_{1,1} = \frac{K}{r}\,\nabla_{\rm s}\widetilde{T}_{1,0}\cdot\nabla_{\rm s}\Psi = -\frac{K}{2\,r}\left[\widetilde{T}_{1,0}\,\Delta_{\rm s}\Psi + \Psi\,\Delta_{\rm s}\widetilde{T}_{1,0} - \Delta_{\rm s}(\widetilde{T}_{1,0}\Psi)\right]. \tag{67}$$

Substituting the series (9) for $\Psi$ and (62) for $\widetilde{T}_{1,0}$, we find

$$\mathcal{E}_{1,1} = -\frac{K}{8\,R\varepsilon_{\rm t}\sigma\,T_0^3}\sum_{j_1\geqslant 1}\sum_{k_1=-j_1}^{j_1}\sum_{j_2\geqslant 1}\sum_{k_2=-j_2}^{j_2} f_{j_1,k_1}\tau_{j_2,k_2}^{(0)}\left[Y_{j_2,k_2}\Delta_{\rm s}Y_{j_1,k_1} + Y_{j_1,k_1}\Delta_{\rm s}Y_{j_2,k_2} - \Delta_{\rm s}(Y_{j_1,k_1}Y_{j_2,k_2})\right]. \tag{68}$$

The action of $\Delta_{\rm s}$ on $\tau_{j_2,k_2}^{(0)}$, where $R$ is a function of spherical harmonics, has been neglected because it generates second order effects.

The next step involves the property of a single spherical harmonic

$$\Delta_{\rm s}Y_{l,m} = -l\,(l+1)\,Y_{l,m}, \tag{69}$$

and the Clebsch–Gordan series for the spherical harmonics product

$$Y_{j_1,k_1}Y_{j_2,k_2} = \sum_{l=\max(|j_1-j_2|,|k_1+k_2|)}^{j_1+j_2}(-1)^{k_1+k_2}\mathcal{G}_{j_1,j_2,l}^{k_1,k_2,-k_1-k_2}\,Y_{l,k_1+k_2}. \tag{70}$$

As the result

$$\mathcal{E}_{1,1} = \frac{\gamma}{R}\sum_{l\geqslant 0}\sum_{j,k,m,p}(-1)^m\,f_{j,k}\tau_{p,m-k}^{(0)}g_{j,p}^{l}\mathcal{G}_{j,p,l}^{k,m-k,-m}\,Y_{l,m}. \tag{71}$$

Now, the rule (60) leads directly to

$$\tau_{l,m}^{(11)} = -(1-A)\,\Phi\,(-1)^m\,\frac{\gamma}{R}\sum_{j\geqslant 1}\sum_{k=-j}^{j} f_{j,k}\sum_{p=0}^{l+j} g_{p,\,j}^{l}\,\mathcal{G}_{p,j,l}^{m-k,k,-m}\sum_{q=-p}^{p}\frac{H_q\,w_{1,p}^{1,q}}{\sigma_{1,1}}\,J_{m-k,q}^{l\,*}(R)\,J_{m-k,q}^{p\,*}(R)\,D_{m-k,q}^{p}. \tag{72}$$

### *4.2.4 Linear solution as the function of a*

Maintaining the first order accuracy with respect to the shape coefficients in our temperature model, we can directly substitute $R = a$ in $\tau_{l,m}^{(1)}$. But the coefficients $\tau_{l,m}^{(0)}$ require more labour and should be linearized with respect to $\Psi$ after the substitution of $R = a(1+\Psi)$. The linear approximation of (63) results in

$$\tau_{l,m}^{(0)} = t_{l,m}^{(0)} + a\,\Psi\,\tau_{l,m}^{(12)}, \tag{73}$$

where

$$t_{l,m}^{(0)} = -(1-A)\,\Phi\sum_{k=-l}^{l}\frac{w_{1,l}^{1,k}\,H_k}{\sigma_{1,1}}\,J_{m,k}^{l\,*}\,D_{m,k}^{l}, \tag{74}$$

$$\tau_{l,m}^{(12)} = -(1-A)\,\Phi\sum_{k=-l}^{l}\frac{w_{1,l}^{1,k}\,H_k}{\sigma_{1,1}}\left(\frac{{\rm d}J_{m,k}^{l\,*}}{{\rm d}a}\right)D_{m,k}^{l}. \tag{75}$$

For the sake of brevity, we adopt a convention that $J_{m,k}^{l}$ without a specified argument stands for $J_{m,k}^{l}(a)$. The factor $\Psi$ in equation (75) is the spherical harmonics series (9). In these circumstances, we resort to the formula (70) to achieve the conversion

$$\sum_{j_1,k_1}\sum_{j_2,k_2} f_{j_1,k_1}\tau_{j_2,k_2}^{(12)}Y_{j_1,k_1}Y_{j_2,k_2} = \sum_{l,m} t_{l,m}^{(12)}Y_{l,m}, \tag{76}$$

with

$$t_{l,m}^{(12)} = -(1-A)\,\Phi\,a\,(-1)^m \sum_{j\geqslant 1}\sum_{k=-j}^{j}\sum_{p\geqslant 1}\sum_{q=-p}^{p} f_{j,k}\,\mathcal{G}_{j,p,l}^{k,m-k,-m}\,\frac{w_{1,p}^{1,q}\,H_q}{\sigma_{1,1}}\,\frac{\mathrm{d}J_{m-k,q}^{p\,*}}{\mathrm{d}a}\,D_{m-k,q}^{p}. \tag{77}$$

An so, finally, the temperature distribution is given in terms of the mean radius $a$ as

$$\varepsilon_\mathrm{t}\,\sigma\,T^4 \approx \varepsilon_\mathrm{t}\,\sigma\,T_0^4 + 4\,\varepsilon_\mathrm{t}\,\sigma\,T_0^3\,(T_{1,0}+T_{1,1}) = \frac{(1-A)\,\Phi}{4} + \sum_{l\geqslant 1}\sum_{m=-l}^{l}\left[t_{l,m}^{(0)} + t_{l,m}^{(1)}\right]\,Y_{l,m}, \tag{78}$$

where $t_{l,m}^{(0)}$ is given by equation (74), and

$$t_{l,m}^{(1)} = (1-A)\,\Phi\,(-1)^m \sum_{j\geqslant 1}\sum_{k=-j}^{j}\sum_{p\geqslant 1}\sum_{q=-p}^{p} f_{j,k}\,\mathcal{G}_{j,p,l}^{k,m-k,-m}\,\frac{w_{1,p}^{1,q}\,H_q}{\sigma_{1,1}}\left[g_{p,j}^{l}\,\left(1-\chi\,J_{m-k,q}^{p\,*}\right)J_{m-k,q}^{l\,*} - a\,\frac{\mathrm{d}J_{m-k,q}^{p\,*}}{\mathrm{d}a}\right]\,D_{m-k,q}^{p}, \tag{79}$$

where the dimensionless quantity $\chi$, known from Vokrouhlický (1999) or Vokrouhlický et al. (2007b),

$$\chi = \frac{\gamma}{a} = \frac{K}{4\,\varepsilon_\mathrm{t}\,\sigma\,T_0^3\,a}, \tag{80}$$

is proportional to the ratio of the thermal parameter and radius of the body scaled by the penetration depth of the thermal wave.

## 5 ELEMENTS OF DYNAMICS

Correcting the sign errors present in section 6 of Breiter & Michalska (2008), we provide the set of equations describing the rotational motion under the action of a general torque $\boldsymbol{M}$. Assuming the circular orbital motion of the rigid body and the alignment of the spin axis with the direction of the maximum moment of inertia, we find

$$\dot{\omega} = \frac{\boldsymbol{M}\cdot\hat{\boldsymbol{e}}_3}{C}, \tag{81}$$

$$\dot{\varepsilon} = \frac{\boldsymbol{M}\cdot\hat{\boldsymbol{e}}_1}{\omega\,C}, \tag{82}$$

$$\dot{\vartheta} = \dot{\psi} = n_\mathrm{s} - \frac{\boldsymbol{M}\cdot\hat{\boldsymbol{e}}_2}{\omega\,C\,s}, \tag{83}$$

$$\dot{\Omega} = -\dot{\phi} = \omega - \frac{c\,\boldsymbol{M}\cdot\hat{\boldsymbol{e}}_2}{\omega\,C\,s} = \omega + c\,(\dot{\vartheta} - n_\mathrm{s}), \tag{84}$$

for the 3-1-3 Euler angles $\Omega = -\phi - \pi/2, \varepsilon, \vartheta = \psi - \pi/2$, and the angular rotation rate $\omega$. $C$ is the maximum moment of inertia, $n_\mathrm{s}$ is the orbital mean motion and, as usual, $c = \cos\varepsilon$, $s = \sin\varepsilon$. The three unit vectors in the above equations define an inertial reference frame attached to the body's equator–equinox system: $\hat{\boldsymbol{e}}_1$, opposite to the projection of $\hat{\boldsymbol{e}}_z'$ (normal to the orbital plane) on the equatorial plane $Oxy$; $\hat{\boldsymbol{e}}_2$, opposite to the vernal equinox (i.e. directed along $\hat{\boldsymbol{e}}_z' \times \hat{\boldsymbol{e}}_z$); and $\hat{\boldsymbol{e}}_3$, directed to the north pole. The components of this right-handed, orthonormal basis in the body frame are given by

$$\begin{aligned}
\hat{\boldsymbol{e}}_1 &= -\cos\phi\,\hat{\boldsymbol{e}}_x - \sin\phi\,\hat{\boldsymbol{e}}_y = -\frac{1}{\sqrt{2}}\,\left[\mathrm{e}^{-\mathrm{i}\phi}\,\hat{\boldsymbol{e}}_+ + e^{\mathrm{i}\phi}\,\hat{\boldsymbol{e}}_-\right],\\
\hat{\boldsymbol{e}}_2 &= \sin\phi\,\hat{\boldsymbol{e}}_x - \cos\phi\,\hat{\boldsymbol{e}}_y = \frac{\mathrm{i}}{\sqrt{2}}\,\left[\mathrm{e}^{-\mathrm{i}\phi}\,\hat{\boldsymbol{e}}_+ - e^{\mathrm{i}\phi}\,\hat{\boldsymbol{e}}_-\right],\\
\hat{\boldsymbol{e}}_3 &= \hat{\boldsymbol{e}}_z,
\end{aligned} \tag{85}$$

where

$$\hat{\boldsymbol{e}}_+ = \frac{1}{\sqrt{2}}\,(\hat{\boldsymbol{e}}_x + \mathrm{i}\,\hat{\boldsymbol{e}}_y) = \hat{\boldsymbol{e}}_-^{\,*}. \tag{86}$$

According to the results of Breiter & Michalska (2008), the YORP torque integrated over the body surface can be approximated as

$$\boldsymbol{M} = \boldsymbol{M}^{(1)} + \boldsymbol{M}^{(02)} + \boldsymbol{M}^{(11)}, \tag{87}$$

where the first order part is

$$\boldsymbol{M}^{(1)} = -\frac{2\,\mathrm{i}\,a^3}{3\,c}\sum_{l\geqslant 1}\sum_{m=-l}^{l} f_{l,m}^{*}\left[\sigma_{l,m}^{-}\,t_{l,m+1}^{(0)}\,\hat{\boldsymbol{e}}_+ + \sigma_{l,m}^{+}\,t_{l,m-1}^{(0)}\,\hat{\boldsymbol{e}}_- + m\,t_{l,m}^{(0)}\,\hat{\boldsymbol{e}}_3\right], \tag{88}$$

and two second order terms read

$$\boldsymbol{M}^{(11)} = -\frac{2\,\mathrm{i}\,a^3}{3\,c}\sum_{l\geqslant 1}\sum_{m=-l}^{l} f_{l,m}^{*}\,[\sigma_{l,m}^{-}\,t_{l,m+1}^{(1)}\,\hat{\boldsymbol{e}}_+ + \sigma_{l,m}^{+}\,t_{l,m-1}^{(1)}\,\hat{\boldsymbol{e}}_- + m\,t_{l,m}^{(1)}\,\hat{\boldsymbol{e}}_3], \tag{89}$$

$$\boldsymbol{M}^{(02)} = \frac{4\,\mathrm{i}\,a^3}{3\,c}\sum_{l,j,p\geqslant 1}\sum_{m=-l}^{l}\sum_{q=-p}^{p} f_{l,m}\,f_{p,q}\left[\sigma_{l,m}^{-}\,\mathcal{G}_{l,p,j}^{m+1,q,-m-q-1}\,t_{j,-m-q-1}^{(0)}\,\hat{\boldsymbol{e}}_- + \sigma_{l,m}^{+}\,\mathcal{G}_{l,p,j}^{m-1,q,-m-q+1}\,t_{j,-m-q+1}^{(0)}\,\hat{\boldsymbol{e}}_+ + m\,\mathcal{G}_{l,p,j}^{m,q,-m-q}\,t_{j,-m-q}^{(0)}\hat{\boldsymbol{e}}_3\right], \tag{90}$$

with auxiliary symbols

$$\sigma_{l,m}^{-}=\sqrt{\frac{(l-m)(l+m+1)}{2}}=\sigma_{l,-m}^{+},\qquad \sigma_{l,m}^{+}=\sqrt{\frac{(l+m)(l-m+1)}{2}}=\sigma_{l,-m}^{-}. \tag{91}$$

Interested in the long-term evolution of the spin axis obliquity $\varepsilon$ and the spin rate $\omega$, we proceed to the expressions of the mean values of $M_3=\boldsymbol{M}\cdot\hat{\boldsymbol{e}}_3$ and $M_1=\boldsymbol{M}\cdot\hat{\boldsymbol{e}}_1$, averaged with respect to both $\phi$ and $\psi$ angles.

## 6 MEAN VALUES OF THE YORP TORQUE PROJECTIONS

Evaluating the mean YORP torque components responsible for the systematic effects in spin rate and obliquity, we can use the formulae derived in section 7 of Breiter & Michalska (2008) that initially depend on the mean values of certain $t_{l,m}^{(0)}$ and $t_{l,m}^{(1)}$ coefficients of the temperature distribution model.

### 6.1 Spin component $M_3$

Similar to the plane–parallel case discussed by Nesvorný & Vokrouhlický (2007, 2008) and Breiter & Michalska (2008), we find that both the first order part of $\langle M_3\rangle$, i.e. $\langle\boldsymbol{M}^{(1)}\cdot\hat{\boldsymbol{e}}_3\rangle$, and the second order $\langle M_3^{(02)}\rangle=\langle\boldsymbol{M}^{(02)}\cdot\hat{\boldsymbol{e}}_3\rangle$ do vanish regardless of the form of $J_{p,q}^{l}$ derived above from the linear temperature model. Thus, the complete $\langle M_3\rangle$ component is equivalent to $\langle M_3^{(11)}\rangle=\langle\boldsymbol{M}^{(11)}\cdot\hat{\boldsymbol{e}}_3\rangle$, and given by the sum

$$\begin{aligned}\langle M_3\rangle &= -\frac{2\,\mathrm{i}\,a^3}{3\,c}\sum_{l\geqslant 1}\sum_{m=-l}^{l} f_{l,m}^{*}\,m\,\left\langle t_{l,m}^{(1)}\right\rangle\\ &= -\mathrm{i}\,\alpha\sum_{l,p,j,m}(-1)^m\,m\,f_{l,m}^{*}\,f_{j,m}\frac{w_{1,p}^{1,0}\,H_0}{\sigma_{1,1}}\,g_{p,j}^{l}\,\mathcal{G}_{l,j,p}^{-m,m,0}\,\mathrm{d}_{0,0}^{p}\left[g_{p,j}^{l}\,\left(1-\chi\,J_{0,0}^{p}\right)J_{0,0}^{l}-a\,\frac{\mathrm{d}J_{0,0}^{p}}{\mathrm{d}a}\right],\end{aligned} \tag{92}$$

where

$$\alpha=\frac{2a^3\,(1-A)\,\Phi}{3c}. \tag{93}$$

Recalling that $H_0=2$, and $w_{1,p}^{1,0}=0$ when $p$ is odd, we reduce $\langle M_3\rangle$ to

$$\langle M_3\rangle=-\mathrm{i}\,2\alpha\sum_{l,j,p\geqslant 1}\sum_{m=-l}^{l}(-1)^m\,m\,f_{l,m}^{*}\,f_{j,m}\,\mathcal{G}_{l,j,2p}^{-m,m,0}\,W_p\,\mathrm{d}_{0,0}^{2p}\left[g_{p,j}^{l}\,\left(1-\chi\,J_{0,0}^{p}\right)J_{0,0}^{l}-a\,\frac{\mathrm{d}J_{0,0}^{p}}{\mathrm{d}a}\right], \tag{94}$$

using the special case of the overlap integral $W_p$ defined by the recurrence

$$W_p=\frac{w_{1,2p}^{1,0}}{\sigma_{1,1}}=\sqrt{\frac{4p+1}{4p-3}}\,\frac{(2p-1)(2p-3)}{2p(2p+2)}\,W_{p-1}, \tag{95}$$

with the initial value $W_0=-\sqrt{\pi}/4$. We also recall that

$$J_{0,0}^{l}=\frac{1}{1+\chi\,l}. \tag{96}$$

Equation (94) can be transformed into a form free of complex quantities:

$$\langle M_3\rangle=\alpha\sum_{l\geqslant 1}\sum_{j\geqslant 1}\sum_{m=1}^{l}(-1)^m\,m\,(C_{l,m}S_{l+2j,m}-S_{l,m}C_{l+2j,m})\sum_{p=j}^{l+j}\mathcal{G}_{l,l+2j,2p}^{-m,m,0}\left(1-\chi\,J_{0,0}^{2p}\right)\left[g_{l,2p}^{l+2j}\,J_{0,0}^{l+2j}-g_{l+2j,2p}^{l}\,J_{0,0}^{l}\right]W_p\,d_{0,0}^{2p}. \tag{97}$$

Note that the terms containing derivatives of the $J$ functions disappeared from this expression.

Finally, we recall it is an advantage to reorganize terms in (97) to give it in explicit series of Legendre polynomials. To that end, we note that $d_{0,0}^{2p}(\varepsilon)=P_{2p}(\cos\varepsilon)$ and we obtain

$$\langle M_3\rangle=\alpha\sum_{q=1}^{N-1}A_q\,P_{2q}(\cos\varepsilon), \tag{98}$$

with

$$A_q=\sum_{j=1}^{q}\sum_{l=l_1}^{N-2j}\tilde{V}_{l,j,q}\sum_{m=1}^{l}S_{l,m}^{j}\,V_{l,m,j,q}, \tag{99}$$

where

$$l_1=\max(1,q-j), \tag{100}$$

and

$$S_{l,m}^{j}=C_{l,m}S_{l+2j,m}-S_{l,m}C_{l+2j,m}, \tag{101}$$

$$V_{l,m,j,q}=m\,(-1)^m\,\mathcal{G}_{l,l+2j,2q}^{-m,m,0}\,W_q, \tag{102}$$

$$\tilde{V}_{l,j,q} = \left(1 - \chi\, J_{0,0}^{2q}\right) \left[g_{l,2q}^{l+2j}\, J_{0,0}^{l+2j} - g_{l+2j,2q}^{l}\, J_{0,0}^{l}\right]. \tag{103}$$

Thus, we factorize $A_q$ into purely numerical $V_{l,m,j,q}$, shape dependent $S_{l,m}^{j}$ and the $\tilde{V}_{l,j,q}$ depending on physical properties of the body – most notably on the thermal conductivity.

### 6.2 Obliquity component $M_1$

The evolution of obliquity $\varepsilon$ is governed by equation (82) and we have to find the mean value of the projection $M_1 = \boldsymbol{M} \cdot \hat{\boldsymbol{e}}_1$. Observing that

$$\hat{\boldsymbol{e}}_+ \cdot \hat{\boldsymbol{e}}_1 = -\frac{\mathrm{e}^{\mathrm{i}\phi}}{\sqrt{2}}, \quad \hat{\boldsymbol{e}}_- \cdot \hat{\boldsymbol{e}}_1 = -\frac{\mathrm{e}^{-\mathrm{i}\phi}}{\sqrt{2}}, \quad \hat{\boldsymbol{e}}_3 \cdot \hat{\boldsymbol{e}}_1 = 0, \tag{104}$$

we find that only the terms factored by $\hat{\boldsymbol{e}}_+$ or $\hat{\boldsymbol{e}}_-$ survive in the torque $\boldsymbol{M}$ projected on $\hat{\boldsymbol{e}}_1$.

#### 6.2.1 First order

Using the first order term $\boldsymbol{M}_1$ defined in equation (88), we obtain

$$\left\langle M_1^{(1)} \right\rangle = \frac{2\,\mathrm{i}\,a^3}{3\sqrt{2}\,c} \sum_{l\geqslant 1} \sum_{m=-l}^{l} f_{l,m}^{*} \left[\sigma_{l,m}^{-} \left\langle t_{l,m+1}^{(0)}\, \mathrm{e}^{\mathrm{i}\phi} \right\rangle + \sigma_{l,m}^{+} \left\langle t_{l,m-1}^{(0)}\, \mathrm{e}^{-\mathrm{i}\phi} \right\rangle\right]. \tag{105}$$

Recalling the definition of $t_{l,m}^{(0)}$, we reject periodic terms by setting $m = 0$ in equation (105) and $k = 0$ in the sum of equation (74). Then, elementary manipulations lead to

$$\left\langle M_1^{(1)} \right\rangle = -\alpha \sum_{l\geqslant 1} C_{l,0}\, \frac{w_{1,l}^{0,1}\, H_0}{\sigma_{1,1}} \sqrt{l(l+1)}\, \mathrm{d}_{1,0}^{l}\, \Im\left(J_{1,0}^{l}\right), \tag{106}$$

where $\Im$ is the imaginary part of a complex expression.

Using the special function $W$ defined in equation (95) and noting the elation between Wigner d-function and the associate Legendre functions

$$\mathrm{d}_{1,0}^{l} = \frac{1}{\sqrt{l\,(l+1)}}\, P_l^1(c), \tag{107}$$

we reduce the mean first order torque component $\langle M_1^{(1)} \rangle$ to the form

$$\left\langle M_1^{(1)} \right\rangle = -2\,\alpha \sum_{l\geqslant 1} C_{2l,0}\, W_l\, P_{2l}^1(c)\, \Im\left(J_{1,0}^{2l}\right), \tag{108}$$

involving only even degree zonal harmonics of the shape model.

#### 6.2.2 Second order

In the second order, we first take the sum of $\hat{\boldsymbol{e}}_1 \cdot \boldsymbol{M}^{(11)}$ and $\hat{\boldsymbol{e}}_1 \cdot \boldsymbol{M}^{(02)}$ using equations (89) and (90). Then, we substitute the temperature coefficients defined in equations (74) and (79). Rejecting periodic terms, we find

$$\left\langle M_1^{(2)} \right\rangle = -\alpha\sqrt{2} \sum_{l\geqslant 1} \sum_{j\geqslant 1} \sum_{m=-l}^{l} \sum_{p\geqslant 0} (-1)^m\, f_{l,m}^{*}\, f_{j,m}\, \mathrm{d}_{1,0}^{2p}\, W_p \left[\sigma_{l,m}^{-}\, \mathcal{G}_{l,j,2p}^{m+1,-m,-1}\, (I_{l,j,p} + \mathrm{i} R_{l,j,p}) + \sigma_{l,m}^{+}\, \mathcal{G}_{l,j,2p}^{m-1,-m,1}\, (I_{l,j,p} - \mathrm{i} R_{l,j,p})\right], \tag{109}$$

where we use the real-valued coefficients $I_{l,p,j}$ and $R_{l,p,j}$ defined by means of

$$R_{l,j,p} + \mathrm{i}\, I_{l,j,p} = 2\, J_{1,0}^{2p} - g_{j,2p}^{l} \left(1 - \chi\, J_{1,0}^{2p}\right) J_{1,0}^{l} + a\, \frac{\mathrm{d} J_{1,0}^{2p}}{\mathrm{d}a}, \tag{110}$$

i.e. as the real and imaginary parts of the right-hand side of (110). A long chain of tedious manipulations involving symmetry properties of and recurrence relations between Gaunt coefficients (Breiter & Michalska 2008) leads to the Legendre series

$$\left\langle M_1^{(2)} \right\rangle = -\alpha \sum_{q=1}^{N} (L_q + N_q)\, P_{2q}^1(\cos\varepsilon), \tag{111}$$

where

$$L_q = \sum_{j=0}^{q} \sum_{l=l_1}^{N-2j} \tilde{X}_{l,j,q} \sum_{m=0}^{l} C_{l,m}^{j}\, X_{l,m,j,q}, \tag{112}$$

$$N_q = \sum_{j=1}^{q} \sum_{l=l_1}^{N-2j} \tilde{Y}_{l,j,q} \sum_{m=1}^{l} S_{l,m}^{j}\, Y_{l,m,j,q}, \tag{113}$$

with shape, thermal properties and numerical factors given by

$$X_{l,m,j,q} = \frac{(-1)^m\, W_q}{2q\,(2q+1)}\,\frac{1+\delta_{0,m}}{1+\delta_{0,j}}\,\mathcal{G}^{m,-m,0}_{l,l+2j,2q}, \tag{114}$$

$$Y_{l,m,j,q} = \frac{(-1)^m\, W_q}{2\sqrt{q\,(2q+1)}}\,\left(\sigma^+_{l,m}\mathcal{G}^{m-1,-m,1}_{l,l+2j,2q} - \sigma^-_{l,m}\mathcal{G}^{m+1,-m,-1}_{l,l+2j,2q}\right), \tag{115}$$

$$\tilde{X}_{l,j,q} = g^{l+2j}_{l,2q}\, I_{l,l+2j,q} + g^{l}_{l+2j,2q} I_{l+2j,l,q}, \tag{116}$$

$$\tilde{Y}_{l,j,q} = (R_{l,l+2j,q} - R_{l+2j,l,q}), \tag{117}$$

$$C^j_{l,m} = C_{l,m}C_{l+2j,m} + S_{l,m}S_{l+2j,m}. \tag{118}$$

Having established the general solution for the YORP effect, valid regardless of the mean radius $a$, we can ask about the limits cases: large body and small body. The approximations will modify the $\tilde{V}_{l,j,q}$, $\Im(J^{2l}_{1,0})$, $\tilde{X}_{l,j,q}$ and $\tilde{Y}_{l,j,q}$ terms.

## 7 LARGE RADIUS APPROXIMATION

According to equation (103), the YORP torque $\langle M_3\rangle$, responsible for the spin rate, depends only on the simple functions $J^p_{0,0}$. For sufficiently large $a$, or – more precisely – for sufficiently small $\chi$, we can use a linearized form

$$J^n_{0,0} \approx 1 - n\chi + O(\chi^2), \tag{119}$$

and – dropping the $O(\chi)$ remainder – we obtain

$$\tilde{V}_{l,j,q} \approx -2j\,(1+2j+2l). \tag{120}$$

This expression is equivalent to the plane-parallel solution given by Breiter & Michalska (2008). We have decided to abandon the term proportional to the first power of $\chi$, because it improves the accuracy only in a very narrow range of $\chi$ values, whereas for larger $\chi$ it seriously degrades the solution quality.

In the obliquity related torque $\langle M_1\rangle$, we need the approximation of functions $J^n_{1,0}$ and their first derivatives. First we have to find the asymptotic approximation of the special case of the general formula (58):

$$J^n_{1,0} = \frac{1}{1+\gamma\, Z_{1,0}\,\frac{j'_n(Z_{1,0}\,a)}{j_n(Z_{1,0}\,a)}}. \tag{121}$$

From now on, we assume that the rotation frequency $\omega$ is strictly positive. This assumption is by no means restrictive, because retrograde rotators will have the obliquity $\varepsilon > \pi/2$ with positive $\omega$. However, assuming $\omega > 0$ we simplify $Z_{1,0}$ that becomes

$$Z_{1,0} = (1+\mathrm{i})\,\sqrt{\frac{\omega}{2\kappa}}. \tag{122}$$

Interestingly, we find that $J^n_{1,0}$ no longer depends on $n$ in the large body limit. An asymptotic expansion leads to[1]

$$J^n_{1,0} \approx \frac{(1+\Theta_1)+\mathrm{i}\,\Theta_1}{Q} + \chi\,\frac{1+2\Theta_1+2\,\mathrm{i}\,\Theta_1\,(1+\Theta_1)}{Q^2} + O(\chi^2), \tag{123}$$

where

$$\Theta_1 = \gamma\sqrt{\frac{\omega}{2\kappa}}, \qquad Q = 1 + 2\,\Theta_1\,(1+\Theta_1). \tag{124}$$

$\Theta_1$ is the thermal parameter known from the heat diffusion theory (see Spencer, Lebofsky & Sykes 1989; Vokrouhlický 1998, 1999; Vokrouhlický et al. 2007b). Differentiating (123), we find another term required in equation (110)

$$a\,\frac{\mathrm{d}J^n_{1,0}}{\mathrm{d}a} \approx -\chi\,\frac{1+2\,\Theta_1+2\,\mathrm{i}\,\Theta_1(1+\Theta_1)}{Q^2}. \tag{125}$$

Substituting the asymptotic approximations into equation (110) and dropping $O(\chi)$ terms, we obtain

$$R_{l,p,j} + \mathrm{i}\,I_{l,p,j} = 2\,J^{2p}_{1,0} - g^l_{j,2p}\,\left(1-\chi\,J^{2p}_{1,0}\right)\,J^l_{1,0} + a\,\frac{\mathrm{d}J^{2p}_{1,0}}{\mathrm{d}a} \approx \left(g^l_{j,2p}-2\right)\,\frac{1+\Theta_1+\mathrm{i}\,\Theta_1}{Q}. \tag{126}$$

Thus, we simplify the coefficients of the obliquity related torque $\langle M_1\rangle$ substituting

$$\Im(J^{2l}_{1,0}) \approx \frac{\Theta_1}{Q} \tag{127}$$

in the first order part (108), and

$$\tilde{X}_{l,j,q} = g^{l+2j}_{l,2q}\, I_{l,l+2j,2q} + g^{l}_{l+2j,2q} I_{l+2j,l,2q} \approx \left[2q\,(2q+1) - g^{l+2j}_{l,2q}\,g^l_{l+2j,2q}\right]\,\frac{2\,\Theta_1}{Q}, \tag{128}$$

[1]Compare with Vokrouhlický (1998), equations (33)–(34).

$$\tilde{Y}_{l,j,q} = (R_{l,l+2j,2q} - R_{l+2j,l,2q}) \approx -2j\,(1+2l+2j)\,\frac{1+\Theta_1}{Q}. \tag{129}$$

And so we recover the results for the plane parallel model from Breiter & Michalska (2008).[2]

## 8 SMALL RADIUS APPROXIMATION

The opposite limit of small bodies is also of great interest, because of the YORP power to modify their rotation state at shorter time-scales. In principle, we know that the YORP torque $\boldsymbol{M}$ itself should vanish for isothermal bodies. Finite conductivity makes the bodies more isothermal at the limit of small size, such that we may want to know exactly how the YORP torque behaves close to $a = 0$.

In the limit of small $a$, or rather $\chi^{-1} \ll 1$, the spin-related functions can be approximated as

$$J^n_{0,0} = \frac{1}{1+n\chi} \approx \frac{1}{n\,\chi} - \frac{1}{(n\,\chi)^2} + O(\chi^{-3}). \tag{130}$$

Quite similar to $J^n_{0,0}$, the functions present in the obliquity related terms have the Maclaurin expansion

$$J^n_{1,0} \approx \frac{1}{n\,\chi} - \frac{1}{(n\,\chi)^2} + O(\chi^{-3}). \tag{131}$$

Note that in this approximation $J^n_{1,0}$ is a real quantity that generates no thermal lag phase. Imaginary part appears at the terms factored by at least $a^3$. The same is true for

$$a\,\frac{\mathrm{d}J^n_{1,0}}{\mathrm{d}a} \approx \frac{1}{n\chi} - \frac{2}{(n\chi)^2} + O(\chi^{-3}). \tag{132}$$

Using the above expressions truncated at $O(\chi^{-1})$, we obtain the simplified version of coefficients

$$\tilde{V}_{l,j,q} \approx \tilde{Y}_{l,j,q} \approx \quad \frac{1}{\chi}\,\frac{j\,(1-2q)\,[(l+j)(1+2l+2j)+q(2q+1)]}{l\,(l+2j)\,q}, \tag{133}$$

$$\Im(J^{2l}_{1,0}) \approx \tilde{X}_{l,j,q} \approx \quad 0. \tag{134}$$

## 9 EXEMPLARY APPLICATION: 1998 KY26

In order to illustrate, the difference between the present solution and previous analytical models, we consider the asteroid 1998 KY26. The YORP effect on this object was studied using numerical methods (Vokrouhlický & Čapek 2002; Čapek & Vokrouhlický 2004), and analytical or semi-analytical models (Nesvorný & Vokrouhlický 2007, 2008; Breiter & Michalska 2008; Scheeres & Mirrahimi 2008). In the present study, we used the shape model of this object expressed in terms of spherical harmonics up to degree and order 100. The same model was used in (Nesvorný & Vokrouhlický 2007, 2008), but only up to degree 24, because increasing the harmonic degree and order in the formulation of Nesvorný & Vokrouhlický (2008) led to serious numerical instability problems.

In all computations, we assumed the following parameters: a circular orbit with major semi-axis 1.23 au, density $\rho = 2800\ \mathrm{kg\,m^{-3}}$, heat capacity $c_p = 680\ \mathrm{J\,kg^{-1}\,K^{-1}}$, emissivity $\varepsilon_\mathrm{t} = 1$, albedo $A = 0$ and the maximum moment of inertia $C = 1.74\,\rho a^5\ \mathrm{kg\,m^2}$, scaled by the density and the fifth power of the mean radius $a$. Whenever the radius remained fixed, we assumed $a \approx 13.176$ m implied by the spherical harmonics expansion of the 4092 triangles model derived from the radar observation by Ostro et al. (1999). Similarly, we took the rotation rate $\omega = 2\pi/642.24\ \mathrm{rad\,s^{-1}}$, unless we used it as an independent variable.

First, we addressed the question of the dependence of the YORP effect on the conductivity of the 1998 KY26. Fig. 2 presents the usual YORP versus obliquity curved with $\dot{\omega}$ plotted to the left, and $\omega\dot{\varepsilon}$ to the right. Both curves were created by means of the general solution. The results for $\omega\dot{\varepsilon}$ fairly well agree with those of Čapek & Vokrouhlický (2004) or Nesvorný & Vokrouhlický (2008), testifying that the plane–parallel model is a good approximation for the attitude dynamics of this particular object. But $\dot{\omega}$ reveals the dependence on conductivity that did not exist in any of the previous models.[3] Compared with the influence on obliquity, it takes much higher conductivity (at least $1\ \mathrm{W\,m^{-1}\,K^{-1}}$) to observe a significant deviation of $\dot{\omega}$ from the Rubincam's approximation. Yet, $K = 1\ \mathrm{W\,m^{-1}\,K^{-1}}$ is still a realistic value (e.g. Delbó et al. 2003).

Since the principal improvement of the previous YORP model consists in accounting for a finite radius, we computed the effect for a family of scaled down KY26-like objects with various radii, starting from a micrometeoroid with $a = 10$ μm, up to $a = 10$ m, assuming a moderate conductivity $K = 0.01\ \mathrm{W\,m^{-1}\,K^{-1}}$. The results are presented in Fig. 3, where we confront the general solution (solid line) with a large body approximation (dotted) and small body limit (dashed). To the left, we present the values of $\dot{\omega}$ for the obliquity $\varepsilon = 0$; to the right, the curves show $|\dot{\varepsilon}|$ at $\varepsilon = 45^\circ$. We marked the part of the solid curve that refers to $\dot{\varepsilon} < 0$ by shading the area below it. In both panels, we see the transition from the large body limit, where the YORP effect is proportional to $a^{-2}$, to the small body limit with the effect proportional to $a^{-1}$. The transition, however, occurs at different radii for the rotation rate and the obliquity evolutions. Moreover, in the intermediate regime,

[2] Apart from a typesetting error in the respective equation (101) of Breiter & Michalska (2008). See also Appendix B of the present paper.

[3] Strictly speaking, Scheeres & Mirrahimi (2008) did introduce a conductivity-dependent factor in the discussion of $\dot{\omega}$ presented in Section 4.3, but their a posteriori correction seems unjustified and incorrect. Note that it depends also on $\omega$ which contradicts the averaged boundary conditions.

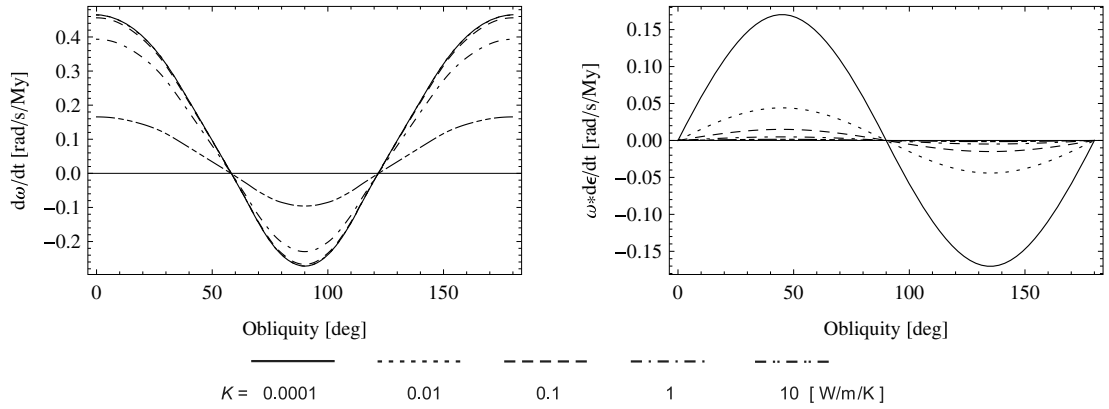


**Figure 2.** Obliquity dependence of the YORP effect for 1998 KY26 with various conductivity values.

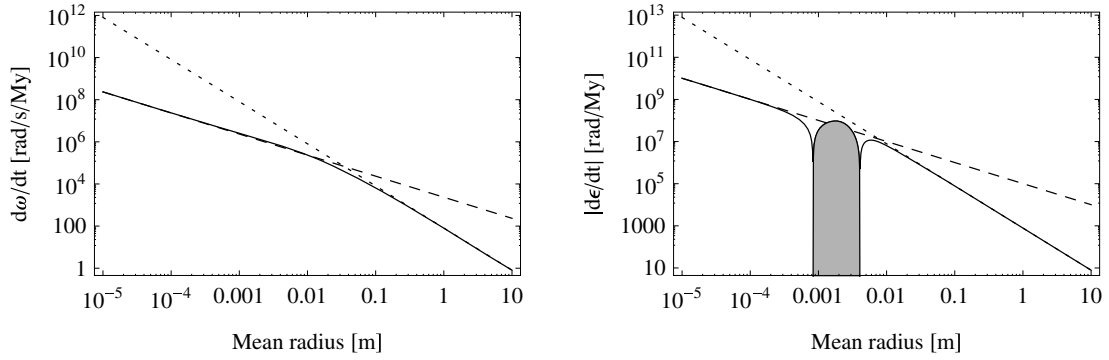


**Figure 3.** Radius dependence of the YORP effect on 1998 KY26 shaped objects. Large body (dotted) and small body (dashed) approximations are confronted with the general solution (solid line). Shaded area refers to the part where $\dot{\varepsilon} < 0$.

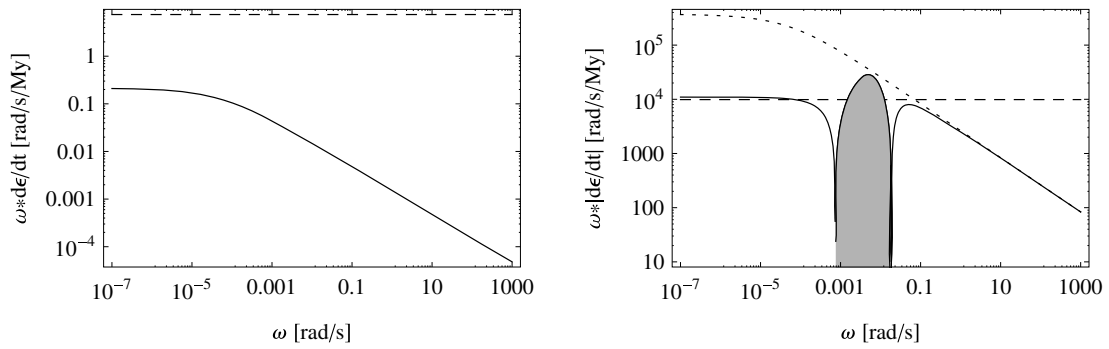


**Figure 4.** Rotation rate dependence of the YORP in obliquity for 1998 KY26. Left: original radius, right: $a = 1$ cm.

the curve of $\dot{\varepsilon}$ as a function of $\varepsilon$ is flipped with respect to the one in Fig. 2. This inversion, occurring without any qualitative change in the shape of $\dot{\omega}$ as a function of obliquity, calls for a new look at the types I and II YORP introduced by Vokrouhlický & Čapek (2002). For example, all type I objects in fig. 11 of Vokrouhlický & Čapek (2002) are characterized by $\dot{\omega} > 0$ at $\varepsilon = 0$, $\dot{\omega} < 0$ at $\varepsilon = 90^\circ$ and $\dot{\varepsilon} \geqslant 0$ for $0 \leqslant \varepsilon \leqslant 90^\circ$. With a new thermal model, we meet the situation where the first two properties are not followed by the third.

In order to understand why the transition occurs at different radii for $\dot{\omega}$ and $\dot{\varepsilon}$, we should inspect the linearization process in Sections 7 and 8. The expansions have been performed according to the magnitude of $a$, but the radius never appears alone. For $\dot{\omega}$ it makes a part of $\chi = \gamma/a$, and indeed, the values of $0.01 < a < 0.1$ m in the case of our test body refer to $0.28 > \chi > 0.028$, when the term $2q\,\chi$ in functions $J^{2q}_{0,0} = 1/(1 + 2q\,\chi)$ is neither a large nor a small parameter for the first few values of $q$. But in the $J^{2q}_{1,0}$ and their derivatives, that appear in $\dot{\varepsilon}$ expressions, $a$ is a factor of the argument $a\,Z_{1,0}$, involving also the rotation rate present in $\Theta_1$. Thus, $a = 0.01$ still refers to $|a\,Z_{1,0}| = 13.6$, and only at $a = 0.001$ the argument drops to $|a\,Z_{1,0}| = 1.36$.

The dependence of the YORP effect on $\omega$ deserves some attention. First, we recall that – within the assumptions of the present solution – the rotation rate related part of the effect is independent on $\omega$. The dependence of $\dot{\varepsilon}$ is twofold: we should distinguish the contribution of $\omega$ in the denominator of equation (82), and the influence of $\omega$ on the torque $\langle M_1 \rangle$. The former is obvious, so Fig. 4 presents only the latter, showing the product $\omega\dot{\varepsilon}$, or – where necessary – its absolute value at $\varepsilon = 45^\circ$. Similar to Fig. 3, we confront the general solution (solid line)

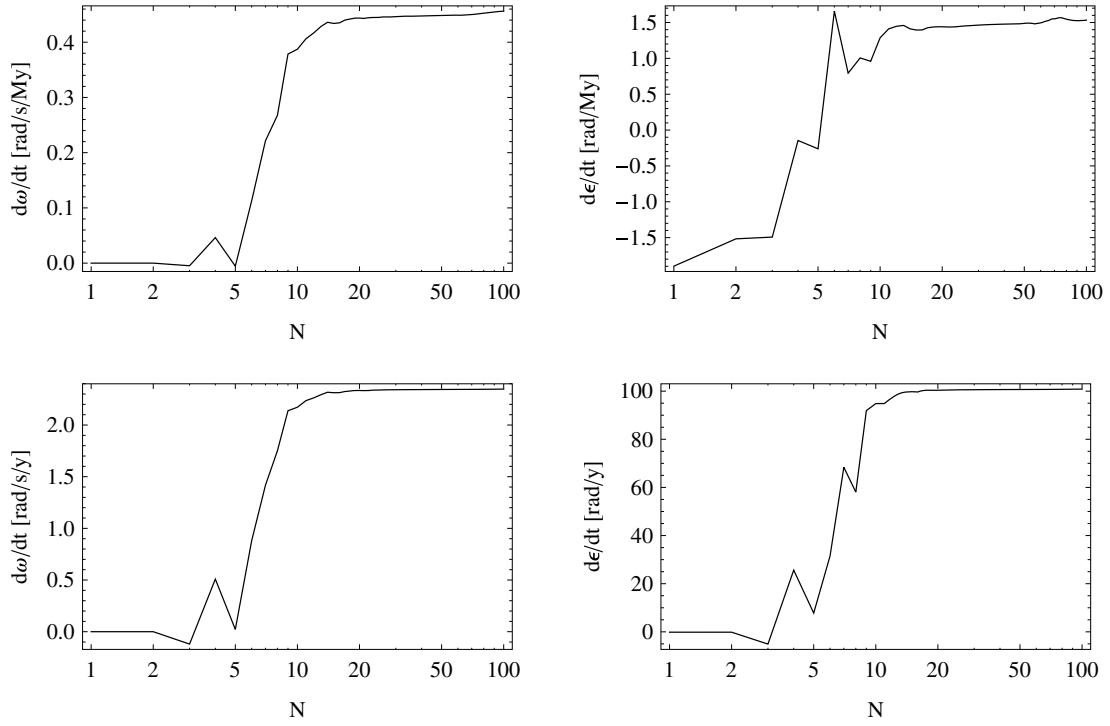


**Figure 5.** YORP effect for 1998 KY26 as a function of the maximum degree of shape harmonics $N$. Top: original radius, bottom: $a = 0.1$ mm.

with the small body limit (dashed) and large body limit (dotted). In this example, we assumed an intermediate value of conductivity $K = 0.1\ \mathrm{W\,m^{-1}\,K^{-1}}$. The most evident feature of Fig. 4, both for the original radius $a \approx 13$ m (left), and for a scaled down object of $a = 0.01$ m, is the presence of two regimes: the torque $\langle M_1 \rangle$ is practically independent on $\omega$ for slow rotators, and inversely proportional to $\omega$ for fast rotators. In other words, $\dot{\varepsilon}$ is proportional to $\omega^{-1}$ for slowly rotating objects, and it turns into the $\omega^{-2}$ proportionality when the rotation rate increases.

Of course, the dependence on $\omega$ is connected with the argument $a\,Z_{1,0}$. For the original size of our test body, the value of $|a\,Z_{1,0}|$ is still as high as 18 for $\omega = 10^{-7}\ \mathrm{rad\,s^{-1}}$. This explains why the large body approximation cannot be distinguished from the general solution in the left-hand panel of Fig. 4, and the small body limit gives completely unrealistic values. But when we pass to a centimetre size object, the argument $|a\,Z_{1,0}|$ takes values between 1.4 and 2 in the shaded zone of the right-hand panel, where none of the approximations is decent.

Finally, Fig. 5 answers the question how many shape harmonics are needed to provide a good approximation of the YORP torque computed according to the present theory with $K = 0.1\ \mathrm{W\,m^{-1}\,K^{-1}}$. Apart from a different behaviour at low $N$, we conclude that shape harmonics up to $N = 20$ provide $\dot{\omega}$ with a relative error of 3 per cent for $a \approx 13$ m and 0.6 per cent for $a = 0.1$ mm. A similar situation is met for $\dot{\varepsilon}$ where the errors are 6 per cent and 0.4 per cent, respectively. However, the 1998 KY26 model provides a smooth surface and its high degree and order harmonics result from the interpolation of a lower resolution triangular mesh. The situation may change for objects with craters and boulders, where the contribution of higher $N$ harmonics should be considerable. Yet, in that case the influence of shadowing is too important to allow a direct application of our theory based upon the spherical terminator approximation.

## 10 CONCLUSIONS

The new analytical model of the YORP effect shares with the previous ones a major part of the limitations. A homogeneous object has been assumed, the shape cannot be too irregular (normal vectors cannot deviate too much from the radial direction). Moreover, surface temperature variations have been linearized and the rotation model excludes not only tumbling, but also any kind of a spin-orbit resonance. Yet, it suppresses two assumptions of previous analytical YORP models: the heat diffusion equation has been solved without assuming an infinite radius, and the boundary conditions account for the deviation of outward normal from the radius vector in the conduction term. The infinite radius has been the assumption not only in analytical, but also in numerical YORP models. As a consequence, there exists no numerical model that might serve as an accuracy test for the present solution. Such a numerical model should be built in the spirit of Spitale & Greenberg (2001), but the extension of their algorithm to non-spherical shapes is a fairly complicated task, especially in the context of the YORP sensitivity to fine details of a body shape (e.g. Statler (2009), Breiter et al. (2009)).

Out of the two improvements, the former (a finite radius) is more important. It allows to inspect the qualitative aspect of the YORP effect for smaller objects. In the Rubincam's approximation or in the large body limit, the YORP torque depends on the radius only through the coefficients $\alpha$, proportional to $a^3$. In the small body limit, the influence of conductivity manifests in making the torque proportional to $a^4$.

Thus, speaking about the torque, we conclude that it tends to 0 with the decreasing radius faster than the previous models suggested.[4] Yet, when it comes to discussing the YORP effect in rotation rate, we have to divide the torque by the maximum moment of inertia proportional to $a^5$ and, conclusions become less comfortable. Even in the small body limit, $\dot{\omega}$ is proportional to $a^{-1}$. This implies that small meteoroids should spin up to unreasonably high, not to say relativistic, angular velocities in quite short time. And even if a non-linear temperature model would additionally damp the thermal YORP torque, the torque due to a scattered light does remain proportional to $a^3$ (see Appendix A), spinning up the bodies at the $a^{-2}$ proportional rate, as it was already proposed by Paddack (1969).

The most probable way out of this catastrophic 'inevitable breakup' scenario is the tumbling rotation state. If the rotation axis migrates away from the principal axis of maximum inertia, we can expect a random walk in obliquity, accompanied by the change of shape harmonics in the new reference frame related to the spin axis. Wandering between positive and negative values of $\dot{\omega}$, a meteoroid can avoid a quick, systematic spin-up. Some (although not all) of the simulated objects in the paper of Vokrouhlický et al. (2007a) indeed followed this scenario.

Interestingly, decreasing the radius, we recover some kind of similarity with the Rubincam's approximation: thermal lag disappears due to the fact that the normal component of temperature gradient becomes very low and can be neglected in the boundary conditions.

In the improved thermal model, we still observe no seasonal YORP effect: unlike in the case of orbital Yarkovsky effect, averaging with respect to the orbital motion leaves no constant part. A similar conclusion resulted from previous analytical and numerical models. The present paper shows that it remains valid even for a finite body temperature distribution.

When conductivity is high, or the radius is small, the influence of finer shape details on the YORP effect becomes reduced. This statement is based not only upon the inspection of Fig. 5, but it also justified by the way the small body limit expressions depend on a harmonic's degree. On the other hand, like all previous conclusions, it has to be preceded by the clause 'within the assumptions of the model'.

## ACKNOWLEDGMENTS

The work of S. Breiter was supported by the Polish Ministry of Science and Higher Education – grant N N203 302535. The work of D. Vokrouhlický was supported by the Czech Grant Agency (grant No. 205/08/0064) and the research program MSM0021620860 of the Czech Ministry of Education.

## REFERENCES

Biedenharn L. C., Louck J. D., 1981, Angular Momentum in Quantum Physics. Addison-Wesley, Reading
Bottke W. F. Jr., Vokrouhlický D., Rubincam D. P., Nesvorný D., 2006, Annu. Rev. Earth Planet. Sci., 34, 157
Breiter S., Michalska H., 2008, MNRAS, 388, 927
Breiter S., Bartczak P., Czekaj M., Oczujda B., Vokrouhlický D., 2009, A&A, in press
Cantrell D. C., 1988, UTD Center for Applied Optics Technical Report No. 8, Numerical Methods for the Accurate Calculation of Spherical Bessel Functions and the Location of Mie Resonances. Univ. Texas at Dallas
Čapek D., Vokrouhlický D., 2004, Icarus, 172, 526
Delbó M., Harris A. W., Binzel R. P., Pravec P., Davies J. K., 2003, Icarus, 166, 116
Nesvorný D., Vokrouhlický D., 2007, AJ, 134, 1750
Nesvorný D., Vokrouhlický D., 2008, AJ, 136, 291
Ostro S. J. et al., 1999, Sci, 285, 557
Paddack S. J., 1969, J. Geophys. Res., 74, 4379
Rubincam D. P., 2000, Icarus, 148, 2
Scheeres D. J., Mirrahimi S., 2008, Celest. Mech. Dyn. Astron., 101, 69
Spencer J. R., Lebofsky L. A., Sykes M. V., 1989, Icarus, 78, 337
Spitale J., Greenberg R., 2001, Icarus, 149, 222
Statler T. S., 2009, Icarus, 202, 502
Vokrouhlický D., 1998, A&A, 335, 1093
Vokrouhlický D., 1999, A&A, 344, 362
Vokrouhlický D., Čapek D., 2002, Icarus, 159, 449
Vokrouhlický D., Breiter S., Nesvorný D., Bottke W. F., 2007a, Icarus, 191, 636
Vokrouhlický D., Nesvorný D., Dones L., Bottke W. F., 2007b, A&A, 471, 717

## APPENDIX A: GENERALIZATION AND COMPUTATIONAL RECIPES

For the readers convenience, we outline the procedure of computing the YORP effect, providing also the generalization for the joint effect of the torques due to the immediate Lambertian scattering of incoming energy flux ($\dot{\omega}_{\rm L}$, $\dot{\varepsilon}_{\rm L}$) and due to the thermal reradiation ($\dot{\omega}$, $\dot{\varepsilon}$). The complete effect is

$$\dot{\omega}_{\rm c} = \dot{\omega} + \dot{\omega}_{\rm L}, \qquad \dot{\varepsilon}_{\rm c} = \dot{\varepsilon} + \dot{\varepsilon}_{\rm L}. \tag{A1}$$

[4]If the body is small, its two opposite points are thermally connected and the resulting gradient becomes nearly linear. We owe this intuitive explanation to the reviewer's comment by Dr. Rubincam.

Obviously, the components obey the same dynamics equations (81) and (82) with the thermal radiation torque $\boldsymbol{M}$ from equation (1) and the scattering torque:

$$\boldsymbol{M}_c = -\frac{2}{3}\frac{A\,\Phi}{c}\oint_S \max\left(0, \hat{\boldsymbol{n}}\cdot\hat{\boldsymbol{n}}_\odot\right)(\boldsymbol{r}\times \mathrm{d}\boldsymbol{S}). \tag{A2}$$

The various levels of approximation that follow are related to the way of handling the thermal radiation component. In all cases, one needs the dimensionless, normalized shape coefficients $C_{l,m}$, $S_{l,m}$, the reference radius of the shape model $a$, the maximum moment of inertia $C$ and the mean power flux $\Phi$ (20) with the orbital semi-axis substituted for $r_0$. Numerical coefficients $V_{l,m,j,q}$, $X_{l,m,j,q}$ and $Y_{l,m,j,q}$ up to $l = N = 100$ and the FORTRAN 77 code computing the thermal YORP can be downloaded from the first author's web page http://vesta.astro.amu.edu.pl/~breiter/YORP2009. $X$ coefficients are not needed for the Rubincam's approximation or the small body model.

### A1 Rubincam's approximation

Unless we are interested in a separate contribution of thermal and scattering terms, albedo $A$ plays no role in the final expressions. So, instead of $\alpha$, we use

$$\alpha_1 = \frac{2\,a^3\Phi}{3c}. \tag{A3}$$

Then, we compute subsequent $F_q$ and $G_q$

$$F_q = -2\sum_{j=1}^{q}\sum_{l=l_1}^{N-2j} j\,(2l+2j+1)\sum_{m=1}^{l} S^j_{l,m}\,V_{l,m,j,q}, \tag{A4}$$

$$G_q = -2\sum_{j=1}^{q}\sum_{l=l_1}^{N-2j} j\,(2l+2j+1)\sum_{m=1}^{l} S^j_{l,m}\,Y_{l,m,j,q}, \tag{A5}$$

where $l_1 = \max(1, q-j)$, and $S^j{}_{l,m}$ is defined in equation (101). Finally,

$$\dot{\omega}_{\mathrm{c}} = \frac{\alpha_1}{C}\sum_{q=1}^{N-1} F_q\,P_{2q}(c), \tag{A6}$$

$$\dot{\varepsilon}_{\mathrm{c}} = -\frac{\alpha_1}{\omega\,C}\sum_{q=1}^{N} G_q\,P^1_{2q}(c), \tag{A7}$$

where $c = \cos\varepsilon$, $P_q$ are Legendre polynomials and $P^1_{2q}$ are associated Legendre functions. If needed, thermal and scattering contributions are easily obtained through the multiplication by $(1-A)$ or $A$, respectively. $F_q$ and $G_q$ serve to compute the scattering terms in all following approximations.

### A2 Small body model

Either we specify the value of $\chi$ or we compute it from equations (80) and (39), given conductivity $K$, albedo $A$ and emissivity $\varepsilon_{\mathrm{t}}$. Then, using equations (99), (101), (113) and (132), we evaluate all $A_q$ and $N_q$. Final expressions are

$$\dot{\omega}_{\mathrm{c}} = \frac{\alpha_1}{C}\sum_{q=1}^{N-1}[(1-A)\,A_q + A\,F_q]\,P_{2q}(c), \tag{A8}$$

$$\dot{\varepsilon}_{\mathrm{c}} = -\frac{\alpha_1}{\omega\,C}\sum_{q=1}^{N}[(1-A)\,N_q + A\,G_q]\,P^1_{2q}(c). \tag{A9}$$

### A3 Large body model

For $\dot{\omega}_{\mathrm{c}}$, the large body model is equivalent to the Rubincam's approximation from Section A1. The effect in obliquity requires the value of $\Theta_1$, computed from density $\rho$, heat capacity $c_{\mathrm{p}}$, conductivity $K$, emissivity $\varepsilon_{\mathrm{t}}$, albedo $A$ and rotation rate $\omega$ using equations (31), (39), (49) and (124). Then, we evaluate $L_q$ and $N_q$ using equations (112), (113), (118), (101), (128), and (129). Numerical coefficients $W_q$ are easily computed from equation (95). Finally, using $G_q$ from Section A1, we obtain

$$\dot{\varepsilon}_{\mathrm{c}} = -\frac{\alpha_1}{\omega\,C}\sum_{q=1}^{N}\left[(1-A)\,\left(2\,C_{2q,0}\,W_{2q}\Theta_1\,Q^{-1} + L_q + N_q\right) + A\,G_q\right]\,P^1_{2q}(c). \tag{A10}$$

### A4 General solution

Given $c_{\rm p}, K, \varepsilon_{\rm t}, A$ and $\omega$, we begin by computing $\gamma, \chi$ and $\Theta_1$ from equations (31), (49), (39) and (124). Numerical coefficients $W_q$ are generated according to equation (95).

The effect in rotation rate requires $F_q$ from Section A1 and $A_q$ defined in equations (99), (100), (101), (103) with $J^n_{0,0} = (1 + n\chi)^{-1}$. Then, $\dot{\omega}_{\rm c}$ is given by equation (A8).

The effect in obliquity is more complicated, because it involves spherical bessel functions and their derivatives. To avoid overflow problems, we use the approach based upon the idea of Cantrell (1988). Given the complex argument $z = a\, Z_{1,0} = (1 + {\rm i})\, \Theta_1/\chi$, we evaluate subsequent

$$w_n = \frac{j_n'(z)}{j_n(z)}, \qquad v_n = \frac{\rm d}{{\rm d}z}\left[\frac{j_n'(z)}{j_n(z)}\right]. \tag{A11}$$

For some high value of $n$, we assume $w_n = v_n = 0$, and follow a stable downward recurrence

$$w_{n-1} = \frac{n-1}{z} - \frac{1}{w_n + (n+1)\, z^{-1}}, \qquad v_{n-1} = -\frac{n-1}{z^2} - \frac{n+1-v_n\, z^{-2}}{(n+1+w_{n-1}\, z)^2}. \tag{A12}$$

The initial value of $n$ should be high enough to guarantee a good accuracy. We take $n = n_1 = \max(|z|,\, 2N + 1)$ as a first guess and then repeat computations starting from $n = 2n_1$. If the difference between $v_{2N}$ or $w_{2N}$ obtained from the two starting values of $n$ is too high, we further increase the initial $n$ until the required accuracy is met.

The complex values $w_n$ and $v_n$ serve to compute the functions

$$J^n_{1,0} = \frac{1}{1 + \chi\, z\, w_n}, \qquad a\, \frac{{\rm d}J^n_{1,0}}{{\rm d}a} = -\chi\, z\, v_n\, \left(J^n_{1,0}\right)^2, \tag{A13}$$

and these, in turn, enter equation (110), serving to compute $\tilde{X}_{l,j,q}$ (116) and $\tilde{Y}_{l,j,q}$ (117), with the definition of $g^l{}_{j,q}$ provided in equation (25). Using equations (101), (112), (113), (108) and (118), we obtain

$$\dot{\varepsilon}_{\rm c} = -\frac{\alpha_1}{\omega\, C} \sum_{q=1}^{N} \left\{(1 - A)\, \left[2\, C_{2q,0}\, W_{2q}\, \Im(J^{2q}_{1,0}) + L_q + N_q\right] + A\, G_q\right\}\, P^1_{2q}(c), \tag{A14}$$

where $G_q$ is defined in Section A1.

## APPENDIX B: ERRATA TO (BREITER & MICHALSKA 2008)

While preparing the present paper, few errors were discovered in the text of Breiter & Michalska (2008). The major point is a wrong relation between the 3-1-3 and 3-2-3 Euler angles, combined with an incorrect definition of vectors $\hat{\boldsymbol{e}}_1,\ \hat{\boldsymbol{e}}_2$. However, the two errors mutually cancel and had no influence on the final YORP effect expressions.

As far as the Euler angles problem is concerned, equations (15) and (16) of the present paper correct the erroneous equations (15), (17) and (A14) in Breiter & Michalska (2008). Fig. 1 is the correct version of fig. 1 from Breiter & Michalska (2008), resolving the issue of $\hat{\boldsymbol{e}}_1,\ \hat{\boldsymbol{e}}_2$. The proper description of these vectors given in Section 5 corrects the text below equation (75) of (Breiter & Michalska 2008).

Equation (101) given by Breiter & Michalska (2008) contains a typographic error. Its correct form can be deduced from the present paper, but in a different notation. Using the symbols from Breiter & Michalska (2008), it should read

$$U^{\rm c}_{l,m,j,p} = (-1)^m\, \frac{2 - \delta_{0,j}}{2 - \delta_{0,m}}\, \left[\frac{g^l_{2p,l+2j}\, g^{l+2j}_{2p,l}}{p\,(2p+1)} - 2\mu\right]\, \mathcal{G}^{m,-m,0}_{l,l+2j,2p}\, W_p.$$

This paper has been typeset from a TEX/LATEX file prepared by the author.